



Mitigating chromatic effects on the transverse focusing of intense charged particle beams for heavy ion fusion [☆]



James M. Mitrani*, Igor D. Kaganovich, Ronald C. Davidson

Princeton Plasma Physics Laboratory, Princeton University, Princeton, NJ 08543, USA

ARTICLE INFO

Available online 3 June 2013

Keywords:

Neutralized drift compression
Solenoid focusing
Chromatic effects

ABSTRACT

A final focusing scheme designed to minimize chromatic effects is discussed. The Neutralized Drift Compression Experiment-II (NDCX-II) will apply a velocity tilt for longitudinal bunch compression, and a final focusing solenoid (FFS) for transverse bunch compression. In the beam frame, neutralized drift compression causes a sufficiently large spread in axial momentum, p_z , resulting in chromatic effects on the final focal spot during transverse bunch compression. Placing a weaker solenoid upstream of a stronger final focusing solenoid (FFS) mitigates chromatic effects, and significantly improves transverse focusing for relevant NDCX-II parameters.

© 2013 Elsevier B.V. All rights reserved.

1. Introduction

One of the challenges for the Neutralized Drift Compression Experiment II (NDCX-II) and heavy ion fusion (HIF) is longitudinally and transversely compressing an intense ion charge bunch in order to maximize fluence and current density on the target [1,2]. Neutralized drift compression [3,4] longitudinally compresses the beam with an induction module applying a variable voltage waveform, which decelerates the particles at the head of the charge bunch, and accelerates the particles at the tail of the charge bunch, resulting in significant longitudinal compression. Due to conservation of phase-space volume, the charge bunch contains a larger spread in axial momentum space, or p_z -space, at the point of longitudinal compression. Unfortunately, a large spread in p_z complicates transverse focusing, as particles with different values of p_z are focused to different axial locations. Therefore, given a large spread in p_z , final focusing schemes for NDCX-II should mitigate chromatic effects to improve transverse focusing [1,5,6]. This paper is organized as follows. Section 2 describes analytical calculations for solenoid focusing using the thin lens approximation; Section 3 shows results of a two-solenoid focusing scheme using relevant NDCX-II parameters; and Section 4 discusses implications of the obtained results.

2. Theoretical model

2.1. Thin lens calculations of solenoid focusing

A brief derivation of solenoid focusing for non-relativistic beams using the thin lens approximation is presented here, in order to analyze chromatic effects on the final focal radius, R_{sp} , and to assist in the design of a final focusing system for relevant NDCX-II parameters. The thin lens approximation allows for compact analytical calculations of emittance and chromatic effects on R_{sp} , where the emittance refers to the unnormalized full transverse emittance of a beam, assuming a Kapchinskij–Vladimirskij (K–V) distribution. For transverse focusing of charged particle beams with solenoids, the thin lens approximation assumes $\kappa \ll 1$, where l is the solenoid length, and $\kappa(z) = qB(z)/2p_z = qB(z)/\sqrt{8MqU}$ is the solenoid force focusing function, and $B(z)$, q , and M are the solenoid's axial magnetic field, ion charge, and ion mass respectively, and $qU = E = p_z^2/2M$ is the ion kinetic energy. Since $\kappa \sim 0.6$ for NDCX-II parameters (Table 1), calculations relying on the thin lens approximation will not yield numerically accurate results. Nevertheless, these calculations do provide a clear picture of the physics behind chromatic effects on transverse focusing.

Solenoid focusing of charged particle beams is well studied [7,8], and is axisymmetric. For non-relativistic axisymmetric, uniform beams with no self-field, the equations of transverse motion are [8]

$$x''(z) - 2\Omega_L(z)y'(z) - \Omega_L'(z)y(z) = 0 \quad (1a)$$

$$y''(z) + 2\Omega_L(z)x'(z) + \Omega_L'(z)x(z) = 0 \quad (1b)$$

where $x(z)$ and $y(z)$ are the particles' transverse position, $\Omega_L(z) = qB(z)/2p_z$ is the normalized Larmor frequency, and primes indicate

[☆]Supported by the U.S. Department of Energy.

* Corresponding author.

E-mail address: jmitrani@pppl.gov (J.M. Mitrani).

Table 1

Experimental parameters used for this study. The “emittance”, ϵ , refers to the unnormalized full transverse emittance of the beam bunch, assuming a K-V distribution. A value of 3 MeV is used for the ion kinetic energy, assuming that NDCX-II has been upgraded for warm dense matter (WDM) studies [1]. The initial radius and angle, R_0 and r'_0 , are assumed to be 30 mm and 0 mrad. The values of B , l , and κ are realistic strength parameters for an NDCX-II final focusing solenoid (FFS) [2], and $\delta E/E$ is the local, peak-to-valley spread in ion kinetic energy at the point of longitudinal compression.

Relevant NDCX-II parameters	
ϵ	2.25 mm mrad
M (Li ⁺ ions)	7 · M _p
R_0	30 mm
B_0 (FFS)	8 T
κ_0 (FFS)	6.04 m ⁻¹
KE	3 MeV
q	+1 e
r'_0	0
l (FFS)	10 cm
$\delta E/E$	20%

derivatives with respect to z . One can simplify Eq. (1) by using the following transformation:

$$X(z) = x(z) \cos \theta_L(z) + y(z) \sin \theta_L(z) \quad (2a)$$

$$Y(z) = -x(z) \sin \theta_L(z) + y(z) \cos \theta_L(z) \quad (2b)$$

where $\theta_L(z) = -\int_{z_0}^z dz' \Omega_L(z')$, to transform to the Larmor frame, and obtain the paraxial ray tracing equation

$$X''(z) = -\kappa(z)^2 X(z) \quad (3a)$$

$$Y''(z) = -\kappa(z)^2 Y(z) \quad (3b)$$

where $[\kappa(z)]^2 = [\Omega_L(z)]^2$, and is defined previously. Under the thin lens approximation, the following derivations will employ the “hard-edge” approximation, where $\kappa(z) = \kappa_0 = qB_0/2p_z$ inside the solenoid and zero outside. Using Eq. (3), particles entering a solenoid with an initial radius R_0 and no initial angle, $r'_0 = 0$, are focused with an angle $r' = -R_0\kappa_0 \sin(\kappa_0 l)$, resulting in a focal length of

$$F = -\frac{R_0}{r'} \approx (\kappa_0^2 l)^{-1}. \quad (4)$$

The emittance-limited final focal radius for beams with finite emittance is [7]

$$R_{sp} \approx \frac{\epsilon F}{R_0}. \quad (5)$$

Because the focal length for solenoids (and quadrupoles) depends on p_z , particles with different values of p_z are focused to different spots on the z -axis. Therefore, solenoids are unable to tightly focus beams with a large spread in p_z , resulting in chromatic effects on R_{sp} . From Fig. 1, the magnitude of the final focal radius, R_{sp} , due to chromatic effects is $\alpha \Delta F$, where α is the angle of approach for particles on the edge of the beam, with energy $E_0 + \delta E/2$, and ΔF is the difference in focal lengths for particles with energy E_0 , and energy $E_0 + \delta E/2$. The first-order approximation, with respect to $\Delta F/F$, of angle α is R_0/F . The relationship $\Delta F \approx (F/E)\Delta E$, where $\Delta E = \delta E/2$ is the difference in kinetic energy between the two particles, can be derived from Eq. (4). Therefore, chromatic effects on R_{sp} for a single solenoid have the form

$$R_{sp} \approx \alpha \Delta F \approx \frac{1}{2} R_0 \frac{\delta E}{E} \quad (6)$$

where $\delta E/E$ is the peak-to-valley spread in ion kinetic energy. When comparing Eqs. (5) and (6), since the ratio of chromatic effects to emittance effects, $(1/2)(R_0 \delta E/E)/(\epsilon F/R_0)$, is > 100 for

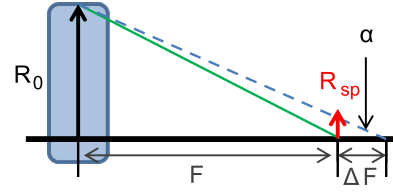


Fig. 1. Schematic, showing chromatic effects on transverse focusing, for a single solenoid. The solid (green) line represents trajectories for particles with energy E_0 , and are focused to a distance F on the z -axis. The dashed (blue) line represents trajectories for particles with energy $E_0 + \delta E/2$, and are focused to a distance $F + \Delta F$ on the z -axis. These particles approach the z -axis with an angle α , which is assumed to be small. In the Figure, the initial beam radius is R_0 , and there is zero initial beam angle. (For interpretation of the references to color in this figure legend, the reader is referred to the web version of this article.)

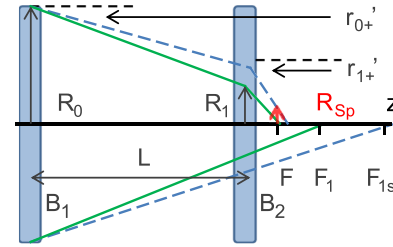


Fig. 2. Schematic, showing chromatic effects on final focusing spot R_{sp} , in a two-solenoid final focusing scheme. Two solenoids, with magnetic field strengths B_1 and B_2 , are separated by a distance L . The solid (green) lines represent a trajectory for a particle with energy E_0 . The solenoid focal lengths for a particle with energy E_0 are F_1 and F_2 [$F \approx (\kappa_0^2 l)^{-1}$, and $\kappa = qB/2p^2$]. The dashed (blue) lines represent a trajectory for a particle with kinetic energy $E_0 + \delta E/2$. Lines below the z -axis represent particle trajectories in the absence of the second solenoid. The solenoid focal lengths for a particle with energy $E_0 + \delta E/2$ are F_{1s} and F_{2s} , where $F_{ns} \approx F_n [1 + (1/2)(\delta E/E)]$, $n=1, 2$. The focal length of both solenoids for a particle with energy E_0 is F , and the resulting focal radius in the presence of two solenoids is labeled R_{sp} . (For interpretation of the references to color in this figure legend, the reader is referred to the web version of this article.)

relevant NDCX-II parameters (Table 1), a final focusing system for NDCX-II should mitigate chromatic effects to improve transverse focusing. In other words, chromatic effects are dominant when the local spread in axial momentum is much larger than the local spread in transverse momentum, $\delta p_z/p_z \gg \delta p_x/p_x, \delta p_y/p_y$, where δp_x and δp_y are due to the transverse emittance, or thermal spread in the beam, and p_x and p_y represent the local transverse beam momentum during transverse compression.

2.2. Thin lens calculations: optimum distance between the two solenoids

Fig. 2 shows particle trajectories in the presence of two solenoids separated by a distance L . The solid (green) line represents trajectories for particles on the edge of the beam with energy E_0 , and the dashed (blue) line represents trajectories for particles with energy $E_0 + \delta E/2$. Lines below the z -axis represent particle trajectories in the absence of the second solenoid. The peak magnetic field strengths are B_1 and B_2 . In Fig. 2, L is slightly less than the focal length of the first solenoid, F_1 , resulting in an underfocused beam entering the second solenoid.

Using the thin lens approximation, the final focal radius in the presence of two solenoids is

$$R_{sp} = R_1 + r'_{1+}(F-L) \quad (7a)$$

$$R_1 = R_0 + r'_{0+}L \quad (7b)$$

$$r'_{0+} = -\frac{R_0}{F_{1s}} \quad (7d)$$

$$r'_{1+} = -\frac{R_0}{F_{1s}} - \frac{R_1}{F_{2s}} \quad (7e)$$

$$F-L = \frac{F_2(F_1-L)}{F_2 + F_1-L} \quad (7f)$$

where R_1 is the radius of the particle orbit with energy $E_0 + \delta E/2$ as it enters the second solenoid; r'_{0+} is the angle of the particle orbit with energy $E_0 + \delta E/2$ as it leaves the first solenoid; r'_{1+} is the angle of the particle with energy $E_0 + \delta E/2$ as it leaves the second solenoid; F_1 and F_2 are the focal lengths for each individual solenoid for the particle with energy E_0 ; F_{1s} and F_{2s} are the focal lengths for the particle with energy $E_0 + \delta E/2$, $F_{ns} = F_n[1 + (1/2)(\delta E/E)]$, $n=1, 2$; and F is the focal length for two solenoids separated by a distance L , for a particle with energy E_0 . By substituting Eqs. (7b)–(7e) into Eq. (7a), and taking the derivative of Eq. (7a) with respect to L , one can show that the optimum distance for transverse focusing for given values of F_1 and F_2 , is given by

$$L_{opt} = F_1 + F_2 - \sqrt{F_1 F_2 + F_2^2} \quad (8)$$

3. Results of the analysis

3.1. Relevant parameters for NDCX-II beams

The parameters relevant to NDCX-II are shown in Table 1. A 3 MeV Li^+ ion beam, with an unnormalized full transverse emittance of 2.25 mm mrad, was assumed. Although NDCX-II will initially be commissioned with 1.2 MeV Li^+ beams, the ion kinetic energy will be increased to 2.8–3.5 MeV in order to study warm dense matter (WDM) [1], so a value of 3 MeV was assumed for this study. The beam is assumed to enter the final focusing solenoid (s) with an initial radius of $R_0=30$ mm, and no initial angle, $r'_0 = 0$. The NDCX-II solenoids will be 10 cm in length, and use copper coils with copper shielding designed to limit magnetic fringe field effects; the form of the assumed axial magnetic field, $B(z)$, is plotted in Fig. 3 [1]. Magnetic field strengths of 8 T and 16 T are considered for the final focusing solenoid. Neutralized drift compression is assumed [3], and self-field effects are neglected in these calculations.

3.2. Numerical calculations of transverse focusing

The preceding analytic derivations assumed a beam with a given initial radius, R_0 , and calculated the final focal radius, R_{sp} , which was assumed to contain 100% of the beam particles. However, a goal for NDCX-II is to maximize particle fluence within set radii. Therefore, the effectiveness of a final focusing system would be better determined by minimizing parameters such as

R_{50} , R_{90} , or R_{100} , the radius containing 50%, 90%, or 100% of the particle fluence, respectively. The half width at half maximum, $hwhm$, is a statistically robust method for comparing radial beam distributions, and is included in this study. In addition to the $hwhm$, the percentage of beam particles within the $hwhm$ is also calculated. That is, a radial density distribution with a narrow $hwhm$ but a low percentage of beam particles within the $hwhm$ will likely have a lower energy density at the target.

The space-charge-free envelope equations provide a numerical estimate of the beam radii under the one- and two-solenoid final focusing schemes. The space-charge-free envelope equations can be obtained from Courant-Snyder theory [9], by substituting the generic solution

$$X_i(z) = A_i w(z) \cos[\psi(z) + \phi_i] \quad (9a)$$

$$Y_i(z) = A_i w(z) \sin[\psi(z) + \phi_i] \quad (9b)$$

into Eq. (3a). The envelope equation is therefore [8]

$$r''(z) = -\kappa(z)^2 r(z) + \frac{e^2}{r(z)^3} \quad (10)$$

and can be used to define the beam radius, assuming a K-V distribution. Because $\kappa(z)$ is a function of beam energy, the envelope equation can only represent one slice in energy space. To account for chromatic effects, Fig. 3 shows plots of three beam envelopes, with energies E_0 and $E_0 \pm \delta E/2$. The dotted black curves in Fig. 3 represent the maximum absolute value of the envelopes, showing visible chromatic effects on transverse focusing.

Radial number density profiles at the focal spot, $n_r(r)$, were numerically calculated by using a Monte-Carlo method to solve many (10^4) individual particle trajectories [Eq. (3)], assuming an initial K-V distribution with a uniform distribution in p_z -space. Using a different initial distribution for the particles' transverse positions and momenta, such as a waterbag or semi-Gaussian distribution, would not yield significantly different results. Approximate estimates of the $hwhm$ and the percentage of beam particles within the $hwhm$ were determined from histograms of $n_r(r)$ (Fig. 4), assuming 25 μm bin widths. The normalized particle fluence at the focal spot is defined as

$$I(r) = \frac{\int_0^r n(r') r' dr' d\theta'}{\int_0^{+\infty} n(r') r' dr' d\theta'} \quad (11)$$

and is used to determine the values of R_{50} , R_{90} , and R_{100} . The results are summarized in Table 2.

A one-solenoid transverse focusing scheme would consist of one strong final focusing solenoid (FFS). Given the beam parameters in Table 1, in the absence of chromatic effects, a single 8 T FFS will focus the beam to a focal radius of ~ 22 μm . However, with a 20% peak-to-valley spread in ion kinetic energy, $\delta E/E$, the final focal radius increases to 3.1 mm. Fig. 5 (dashed lines) shows that increasing the magnetic field strength of the FFS has a negligible effect on the final focus radius.

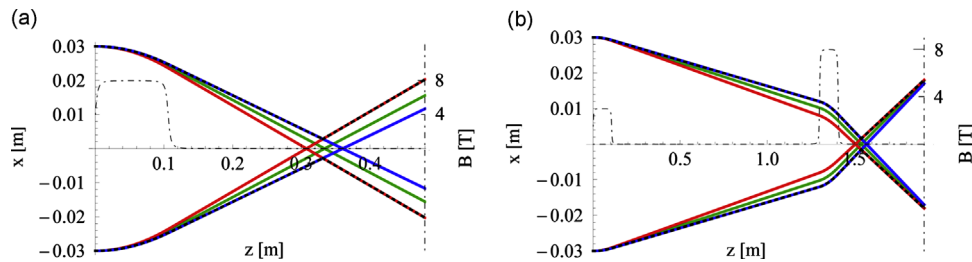


Fig. 3. The green, blue, and red envelopes represent three beam slices, where the beam energy is E_0 , $E_0 + \delta E/2$, and $E_0 - \delta E/2$, $E_0=3$ MeV, and $\delta E/E=0.2$. The dashed gray curves represent the form of $B(z)$ used for the solenoids' axial magnetic field. The effective lengths of the solenoids, $l = B_0^2 \int dz B^2(z)$ [7], are 10 cm. (a) One final focusing solenoid scheme, where $B=8$ T. (b) Two-solenoid scheme, where $B_1=3$ T, and $B_2=8$ T. The solenoids are separated by a distance of $L=1.3$ m. (For interpretation of the references to color in this figure legend, the reader is referred to the web version of this article.)

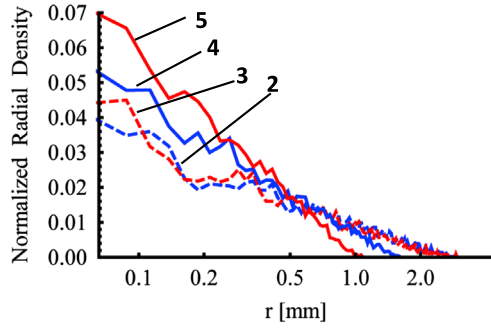


Fig. 4. Normalized radial density plots at the focal spot, $n_r(r)$, for a one-solenoid final focusing scheme (dotted lines), and for a two-solenoid final focusing scheme (solid lines). Plots labeled 2 (blue) and 3 (red), represent normalized radial density plots under the one-solenoid final focusing scheme, for $B=8$ T and $B=16$ T, respectively. Plots labeled 4 (blue), and 5 (red) represent normalized radial density plots under the two-solenoid final focusing scheme, for $B_1=3$ T and $B_2=8$ T, and $B_1=3$ T and $B_2=16$ T, respectively. (For interpretation of the references to color in this figure legend, the reader is referred to the web version of this article.)

Table 2

Results from Monte-Carlo calculations under the one- and two-solenoid final focusing schemes. For the two-solenoid final focusing scheme, magnetic field strengths of $B_1=3$ T and $B_2=8$ T, and $B_1=3$ T and $B_2=16$ T are considered. The value of $hwhm$ was roughly estimated from histograms, with $25 \mu\text{m}$ bin widths, of the radial density distribution, $n_r(r)$ (Fig. 4). The percentage of beam particles within the $hwhm$ is also included. The values of R_{50} , R_{90} , and R_{100} , are the radii containing 50%, 90%, and 100% of the normalized fluence, respectively. The distance L between the two solenoids is $L=1.3$ m for $B_2=8$ T, and $L=1.6$ m for $B_2=16$ T.

Results	One solenoid			Two solenoids	
B_1 (T)				3	3
B-field (T)	3	8	16	8	16
$hwhm$ (mm)	0.43	0.43	0.35	0.28	0.18
$hwhm$ (%)	41	44	42	49	47
R_{50} (mm)	1.2	1.2	1.1	0.66	0.41
R_{90} (mm)	2.3	2.2	2.1	1.2	0.76
R_{100} (mm)	3.3	3.1	3.0	1.6	1.1

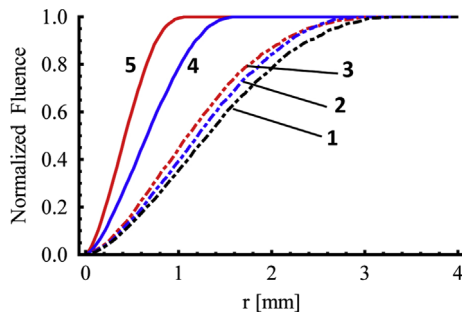


Fig. 5. Normalized particle fluence plots [Eq. (11)] at the focal spot, for a one-solenoid final focusing scheme (dotted lines), and for a two-solenoid final focusing scheme (solid lines). Plots labeled 1 (black), 2 (blue), and 3 (red) represent fluence plots under the one-solenoid final focusing scheme, for $B=3$ T, 8 T, and 16 T, respectively. Plots labeled 4 (blue), and 5 (red) represent fluence plots under the two-solenoid final focusing scheme, for $B_1=3$ T and $B_2=8$ T, and $B_1=3$ T and $B_2=16$ T, respectively. (For interpretation of the references to color in this figure legend, the reader is referred to the web version of this article.)

Figs. 3(b) and 5 (solid lines) show that the two-solenoid scheme significantly improves transverse focusing. The optimum distance, L , between the two solenoids was analytically calculated using the thin lens approximation [Eq. (8)], and numerically calculated using finite lens lengths (Fig. 6). The results are compared in Table 3. In the two-solenoid scheme, given NDCX-II parameters, the focal length of the first $B_1=3$ T solenoid is ~ 2 m. Therefore, the beam is

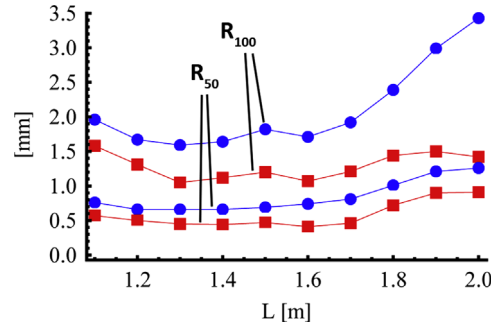


Fig. 6. Values of R_{50} and R_{100} with varying values for the distance, L , between the two solenoids, in a two-solenoid final focusing scheme. B_1 is fixed at 3 T, for all data points shown in the figure. The value of B_2 is 8 T for the circle (blue) points, and $B_2=16$ T for the square (red) points. From the above graph, the optimum values for L are $L=1.3$ m for $B_2=8$ T, and $L=1.6$ m for $B_2=16$ T. [Eq. (8) gives values of $L=1.45$ m for $B_2=8$ T, and $L=1.63$ m for $B_2=16$ T.] All other values are the same as in Table 1. (For interpretation of the references to color in this figure legend, the reader is referred to the web version of this article.)

Table 3

Optimum distance, L , between the solenoids, for the two-solenoid final focusing scheme. The value of B_1 is fixed at 3 T, and all parameters are in Table 1. Note that Eq. (8) relies on the thin-lens approximation, whereas Fig. 6 uses finite lens lengths.

Two-solenoid final focusing scheme optimum distance, L		
B_2 (T)	8	16
Eq. (8) (m)	1.45	1.63
Fig. 6 (m)	1.3	1.6

underfocused before entering the second solenoid. Reducing the magnetic field strength of the first solenoid, B_1 , would increase the focal length, and increase the spatial requirements for a two-solenoid final focusing scheme. Fig. 5 compares the normalized particle fluence [Eq. (11)] for the one- and two-solenoid schemes, showing a significant improvement in transverse focusing for the two-solenoid scheme for $B_2=8$ T, and $B_2=16$ T. Table 2 shows that the two-solenoid scheme increases particle fluence, measured by R_{50} , R_{90} , and R_{100} , by a factor of ~ 2 for an 8 T final focusing solenoid. The results for a 16 T final focusing solenoid are even better, as the two-solenoid scheme increases particle fluence, measured by R_{50} , R_{90} , and R_{100} , by a factor of ~ 3 .

4. Discussion

A two-solenoid final focusing scheme mitigates chromatic effects, resulting in a smaller final focal radius, R_{sp} . Equation (5) shows that in the absence of chromatic effects, the final focal radius R_{sp} is inversely proportional to R_0 . However, in the presence of strong chromatic effects, the value of R_{sp} is roughly proportional to R_0 [Eq. (6)], and decreasing the initial beam radius before the beam enters the final focusing solenoid leads to a smaller focal spot. Effects such as radial misalignments, emittance growth [10], coupling between transverse and longitudinal emittance [11], or other effects that limit longitudinal compression [12,13] were not considered in this study.

We have proposed using a two-solenoid focusing scheme for beams with relevant NDCX-II parameters. Neutralized drift compression was assumed, resulting in a narrow beam distribution in z -space, and a large spread in p_z -space, at the point of maximum longitudinal compression. For beams with a sufficiently large spread in p_z , the two-solenoid focusing scheme significantly improves transverse focusing relative to a one-solenoid final focusing scheme.

Acknowledgments

This research was supported by the U.S. Department of Energy under Contract DE-AC02-09CH11466. The authors would like to thank Erik Gilson, for fruitful discussions.

References

- [1] A. Friedman, et al., *Physics of Plasmas* 17 (2010) 056704.
- [2] P. Seidl, et al., *Nuclear Instruments and Methods in Physics Research Section A* 606 (2009) 75.
- [3] P. Roy, et al., *Physical Review Letters* 95 (2005) 234801.
- [4] D. Welch, et al., *Nuclear Instruments and Methods in Physics Research Section A* 544 (2005) 236.
- [5] J. Barnard, et al., in: *Proceedings of the 2005 Particle Accelerator Conference*, Knoxville, TN, p. 2568.
- [6] W. Sharp, et al., *Nuclear Instruments and Methods in Physics Research Section A* 606 (2009) 97.
- [7] M. Reiser, *Theory and Design of Charged Particle Beams*, Wiley, New York, 1994.
- [8] R. Davidson, H. Qin, *Physics of Intense Charged Particle Beams in High Energy Accelerators*, World Scientific, Singapore, 2001.
- [9] E. Courant, H. Snyder, *Annals of Physics* 3 (1958) 1.
- [10] E. Gilson, et al., *Physics of Plasmas* 17 (2010) 056707.
- [11] H. Qin, et al., in: *Proceedings of the 2011 Particle Accelerator Conference*, New York, NY, p. 758.
- [12] I. Kaganovich, et al., *Nuclear Instruments and Methods in Physics Research Section A* 678 (2012) 48.
- [13] A. Sefkow, R. Davidson, *Physical Review Special Topics* 10 (2007) 100101.